FAST SUPER-RESOLUTION ACOUSTIC IMAGING FOR UNDERWATER DISTRIBUTED ACOUSTIC SENSING USING IMPROVED RICHARDSON–LUCY DECONVOLUTION

Jie Wu[1], Changxin Fa[2], Huayong Yang[1]
[1] *Southern Marine Science and Engineering Guangdong Laboratory (Guangzhou), Guangzhou 511458, China*
[2] *National Key Laboratory of Underwater Acoustic Technology, Harbin 150001, China*

Abstract

Distributed acoustic sensing (DAS) transforms optical fibers into dense underwater acoustic arrays, but conventional beamforming produces broad mainlobes and strong sidelobes when coherent near-field sources are present. This paper develops a compact super-resolution imaging framework based on improved Richardson–Lucy (RL) deconvolution. A conventional near-field delay-and-sum image is first generated from the DAS channels. A position-dependent point-spread function (PSF) dictionary is then constructed and vectorized, after which a non-negative RL iteration reconstructs the source distribution. For dense DAS data, spatial resampling and matrix-form dictionary operations reduce the number of active channels and avoid repeated four-dimensional PSF indexing. The method is evaluated through numerical simulations, an anechoic tank experiment with two coherent 950-Hz sources, and a Danjiangkou lake experiment in which a UUV crossed a section of a 1-km-long lakebed fiber. The results show super-Rayleigh separation of coherent sources, an approximately 60% reduction in mainlobe width, sidelobe suppression exceeding 10 dB, and reconstructed range errors below 0.2 m in the tank experiment. The approach provides a simple and efficient route to high-resolution underwater DAS imaging without relying on subspace decomposition or a pre-estimated source range.

Keywords: *distributed acoustic sensing, underwater acoustic imaging, improved Richardson–Lucy deconvolution, near-field localization, UUV detection*

Corresponding author: *wu_jie@gmlab.ac.cn.*

1. Introduction

Phase-sensitive optical time-domain reflectometry converts an optical fiber into a continuously sampled acoustic aperture. Compared with discrete hydrophone arrays, distributed acoustic sensing (DAS) provides flexible digital channel selection, a potentially large physical aperture, and kilometer-scale coverage without local electrical power along the sensing cable [1]–[4]. These properties are attractive for underwater monitoring and moving-target detection. However, dense spatial sampling also produces large data volumes, while the effective cable geometry and acoustic propagation conditions may vary along the array.

Near-field imaging is particularly difficult because the incident wavefront is spherical and the beam response varies with source position. For coherent narrowband sources, conventional delay-and-sum beamforming (DAS-BF) often produces a broad coupled mainlobe and high sidelobes. Subspace and covariance-fitting methods can improve angular resolution, but their outputs and assumptions differ from direct acoustic imaging..

This paper addresses a different inverse problem. The conventional two-dimensional DAS-BF image is treated as a blurred observation, and a position-dependent PSF dictionary is used in an improved RL deconvolution to recover the spatial source distribution. The proposed method does not form a sample covariance matrix, does not require a TDOA-derived range estimate, and directly outputs a Cartesian or range–bearing image. It nevertheless requires a prescribed scan region and a calibrated or nominal array geometry for PSF construction. The main contributions are:

1. a position-dependent PSF model for near-field DAS imaging, which accounts for the spatially varying beam response instead of assuming a shift-invariant convolution kernel;

2. a vectorized non-negative RL reconstruction framework combined with spatial resampling, enabling efficient processing of densely sampled DAS channels;

3. comprehensive validation through numerical simulations, a coherent-source anechoic-tank experiment, and a moving-UUV lake experiment with a 1-km lakebed DAS cable.

2. Improved RL Imaging Method

2.1. Near-field DAS image formation

Consider a two-dimensional imaging plane containing the selected DAS aperture and candidate source positions. Let the mth retained DAS channel be located at $\mathbf{r}_m$, and let $\mathbf{r} = (x, y)$ denote a candidate source position. The propagation delay relative to the reference channel is

$$\tau_m(\mathbf{r}) = \frac{\|\mathbf{r} - \mathbf{r}_m\| - \|\mathbf{r} - \mathbf{r}_{\mathrm{ref}}\|}{c}, \tag{1}$$

where c is the sound speed and $\mathbf{r}_{\mathrm{ref}}$ is the reference-channel position. For frequency-domain data $X_m(f)$, the band-integrated near-field delay-and-sum image is

$$B(\mathbf{r}) = \int_{\mathcal{F}} \left| \sum_{m\in\mathcal{M}} w_m X_m(f) \exp[j2\pi f \tau_m(\mathbf{r})] \right|^2 \mathrm{d}f, \tag{2}$$

where $\mathcal{F}$ is the processing band, $\mathcal{M}$ is the retained channel set, $M_s = |\mathcal{M}|$, and w_m is the channel weight. Uniform weights, $w_m = 1/M_s$, are used in the reported results. The same analysis frame, preprocessing, channel set, sound-speed value, and scan grid are used for both the conventional image and PSF generation. Because the focusing delay and effective aperture vary across the scan region, the resulting PSF is position dependent.

For each candidate source pixel v, a unit source is simulated or calibrated at position $\mathbf{r}_v$ and processed using the same beamformer. Its response at image pixel u defines the PSF element $p(u \mid v)$. Each PSF column is normalized to unit ℓ_1 norm. After vectorizing the conventional image and the PSF images, the approximate image-domain model is

$$\mathbf{b} \approx \mathbf{P}\mathbf{q} + \mathbf{e}, \tag{3}$$

where $\mathbf{b} \in \mathbb{R}_+^U$ is the vectorized DAS-BF image, $\mathbf{P} \in \mathbb{R}_+^{U\times V}$ is the position-dependent PSF dictionary, $\mathbf{q} \in \mathbb{R}_+^V$ is the unknown spatial source distribution, and $\mathbf{e}$ contains noise and model mismatch. For coherent sources, cross terms in the beamformer power image prevent exact linear superposition. Equation (3) is therefore an image-domain approximation, and the RL iteration is used as a non-negative reconstruction operator rather than an exact coherent-field inverse.

2.2. Non-negative RL reconstruction

The Richardson–Lucy method was originally developed for non-negative image restoration [5], [6]. With an elementwise positive initialization $\mathbf{q}^{(0)}$, the matrix-form update is

$$\mathbf{q}^{(k+1)} = \mathbf{q}^{(k)} \odot \frac{\mathbf{P}^{\mathrm{T}} \left[\mathbf{b} \oslash \left(\mathbf{P}\mathbf{q}^{(k)} + \varepsilon \mathbf{1} \right) \right]}{\mathbf{P}^{\mathrm{T}}\mathbf{1} + \varepsilon \mathbf{1}}, \tag{4}$$

where $\odot$ and $\oslash$ denote elementwise multiplication and division, respectively, and ε is a small positive constant used only to prevent division by zero. Before iteration, $\mathbf{b}$ is normalized by its maximum value, and a spatially uniform positive vector is used for $\mathbf{q}^{(0)}$. The update preserves non-negativity and does not require covariance decomposition or the source number as an input. A fixed iteration count is used for consistent processing, with $K = 200$ for all reported simulation, tank, and lake results. Although the image-domain error does not strictly follow a Poisson distribution, the multiplicative RL update provides a practical non-negative deconvolution procedure.

2.3. Spatial resampling and matrix implementation

Let the original DAS channel spacing be d_0 and let S denote an integer spatial-resampling factor. The retained spacing is $d_s = Sd_0$, and the retained channels are distributed across the original physical aperture. The PSF dictionary is generated for exactly the same retained channel set. Spatial resampling reduces the number of active channels and hence the beamforming workload, while the physical aperture is preserved as far as the selected channel distribution permits. Excessive resampling may introduce spatial aliasing or grating responses and must therefore be constrained by the operating band and array geometry.

The four-dimensional PSF description $p(x, y \mid X, Y)$ is reorganized into the matrix $\mathbf{P}$, while the conventional image is vectorized into $\mathbf{b}$. For U image samples, V candidate source pixels, and K iterations, the dominant RL cost is $\mathcal{O}(KUV)$. The dictionary is precomputed offline, and the online iterations use matrix–vector operations rather than repeated four-dimensional indexing. Thus, the term "fast" refers to reduced active-channel processing and matrix implementation; no real-time processing claim is made in this paper. If the cable geometry, sound-speed model, or operating band changes substantially, the PSF dictionary must be recalibrated.

2.4. Evaluation metrics

The normalized spatial-response cut through each reconstructed source peak is used for quantitative comparison. The mainlobe width $W_{-3\mathrm{dB}}$ is defined by the two -3 dB crossing points. The relative mainlobe reduction is

$$\rho_W = 1 - \frac{W_{-3\mathrm{dB}}^{\mathrm{RL}}}{W_{-3\mathrm{dB}}^{\mathrm{CBF}}}. \tag{5}$$

The peak sidelobe level is defined as

$$\mathrm{PSL} = 10 \log_{10} \frac{\max_{u\in\Omega_{\mathrm{SL}}} I(u)}{I_{\max}}, \tag{6}$$

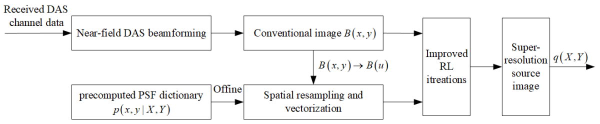

Figure 1: Processing flow of the proposed image-domain DAS reconstruction method.

where $I_{\max}$ is the main-peak value and Ω_{SL} excludes the mainlobe between its -3 dB crossings. The reconstructed range error is $e_r = |\hat{r} - r_0|$, where r_0 is the measured reference range. Here, super-Rayleigh separation refers to resolving two sources that appear as a single mainlobe in the conventional CBF image under the same array-aperture and frequency settings.

3. Numerical Simulation and Tank Experiment

3.1. Numerical Simulation

A 21-element linear array with 2-m spacing is simulated over the Cartesian scan region $x \in [-10, 10]$ m and $y \in [10, 40]$ m. The source frequency is 600 Hz, the additive noise is limited to 400–800 Hz, and the in-band SNR is 15 dB, where SNR is calculated from the signal and noise powers within the processing band. The beamforming image and every PSF column use the same Cartesian grid. Three cases are examined: a single source at $(0, 26)$ m; two equal-strength coherent sources at $(-1, 26)$ m and $(0.6, 22.8)$ m; and the same double-source geometry with a 3 dB source-level difference. The RL iteration number is $K = 200$.

As shown in Fig. 2, the reconstructed images retain the source positions while concentrating the conventional beamforming response into compact peaks. The two close sources remain separable in both the equal- and unequal-strength cases. The simulation verifies the position-dependent dictionary and non-negative reconstruction under controlled conditions; it is not intended as a complete Monte Carlo robustness analysis.

3.2. Tank Experiment

The tank recordings were acquired at Harbin Engineering University using two coherent 950-Hz continuous-wave sources at a depth of 2.5 m. The receiving fiber formed an eight-channel DAS array at a depth of 5 m. The channel spacing was 0.64 m, the gauge length was 5 m, the DAS temporal sampling rate was 20 kHz, and the interrogator pulse duration was 50 μs. The horizontal source-to-array separation was approximately 13.4 m. The same selected channels and nominal geometry were used to generate both the conventional image and position-dependent PSF dictionary.

The measured tank data are processed using conventional near-field beamforming followed by the proposed position-dependent RL reconstruction. The experiment is designed to assess whether the method can separate two coherent near-field sources and suppress the broad mainlobe and sidelobe structures produced by conventional beamforming. The performance is

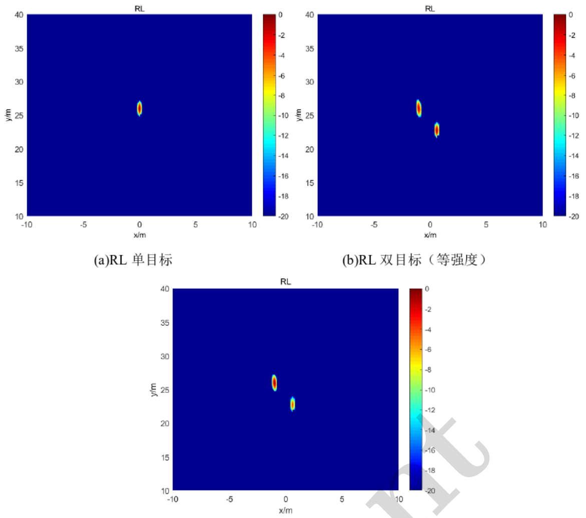

Figure 2: RL reconstructions for the single-source and coherent double-source simulations.

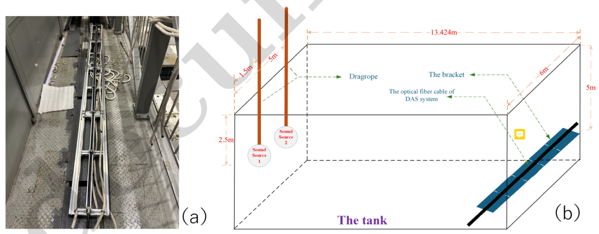

Figure 3: Configuration of the shared coherent-source DAS tank dataset.

evaluated in terms of image mainlobe width, peak sidelobe level, source-peak separation, and reconstructed source range.

The conventional image contains a broad coupled response and does not provide two clearly separated peaks. The RL reconstruction produces two compact peaks, providing super-Rayleigh separation in the operational sense defined in Section 2. For the representative spatial cuts, the -3 dB mainlobe width is reduced by approximately 60%, and the peak sidelobe level is improved by more than 10 dB. The measured reference ranges are 13.63 and 14.00 m, whereas the reconstructed peaks are located near 13.5 and 14.0 m, giving representative range errors below 0.2 m. These results apply to the present array geometry, frequency, selected frame, and PSF calibration and should not be generalized without further experiments.

4. Danjiangkou Lake Experiment

A moving-target experiment was conducted near Songgang Wharf in the Danjiangkou Reservoir on 14 May 2025. As illustrated in Fig. 5, the local water depth was approximately 40 m, and a 1-km DAS cable extended from the shore-based interrogator along the lakebed. At 16:23:27, a UUV supplied by Northwestern Polytechnical University entered the water and

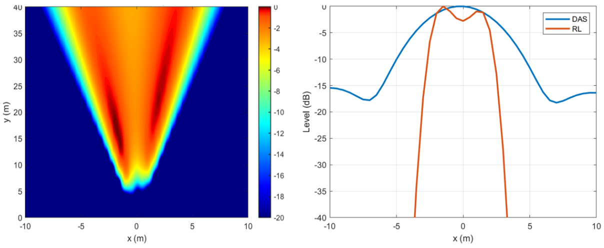

Figure 4: Representative tank-data comparison between conventional beamforming and improved RL reconstruction.

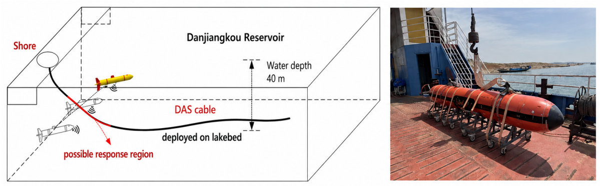

Figure 5: Danjiangkou DAS–UUV lake experiment: (a) schematic of the lakebed DAS-cable deployment and planned UUV crossing route; (b) UUV platform used in the experiment.

travelled at approximately 5 kn along a predefined route. The vehicle crossed the cable from the side and subsequently moved away from the sensing region. The UUV was approximately 4 m long and 533 mm in diameter. During submerged operation, it relied on onboard inertial navigation, while GPS was used for route correction after resurfacing.

The lake-trial DAS data were sampled at 4 kHz. A local aperture comprising channels 380–430 was selected, giving 51 DAS channels, and the processing band was restricted to 800–840 Hz. A locally straight nominal cable section was adopted for near-field focusing and PSF construction because the detailed three-dimensional lakebed-cable shape was unavailable. The representative waveform in Fig. 6(a) is taken from a channel near the centre of the selected aperture; it is shown only to illustrate the temporal variation of the received signal. The conventional beamforming and RL images use all 51 selected channels. The spectrogram in Fig. 6(b) shows time-varying energy in the 800–840-Hz processing band during the UUV passage. Because no synchronized underwater ground-truth trajectory is available, this energy variation is not used alone to infer the instantaneous UUV–cable distance.

The 51-channel data were processed frame by frame using conventional near-field beamforming and the proposed RL reconstruction. Figure 6(c) contains broad distance–direction responses and pronounced sidelobe structures, making the dominant target-related components difficult to isolate. After RL reconstruction, Fig. 6(d) presents a sparser spatial distribution in which diffuse responses are suppressed and several localized high-energy components are retained. These localized responses are interpreted as potential target-

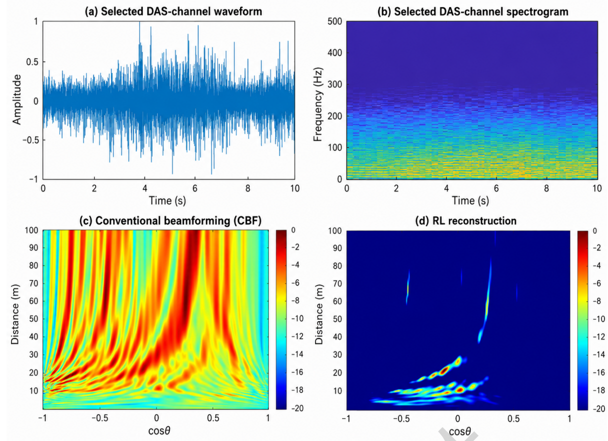

Figure 6: Processing results of the Danjiangkou UUV experiment using DAS channels 380–430 and the 800–840-Hz band: (a) waveform of a representative channel; (b) corresponding spectrogram; (c) conventional beamforming result; and (d) RL reconstruction.

related components rather than as a directly validated UUV trajectory.

The lake experiment demonstrates that the image-domain deconvolution can be applied to moving-source data acquired with a kilometer-scale underwater DAS deployment. Compared with conventional beamforming, the RL result provides stronger suppression of diffuse responses and a more concentrated representation of potential UUV response regions. The 1-km value describes the deployed cable length rather than the effective aperture used for imaging; only channels 380–430 are included in the reported result. Because the exact underwater UUV trajectory and detailed lakebed-cable geometry are unavailable, the lake data are used to demonstrate moving-target detectability and practical applicability, not to report absolute trajectory-localization error.

5. Conclusion

A super-resolution acoustic imaging method for underwater DAS has been developed using position-dependent Richardson–Lucy deconvolution. A conventional near-field image is represented by a spatially varying PSF dictionary, and a non-negative matrix-form iteration reconstructs the two-dimensional source distribution. Spatial resampling reduces the number of active DAS channels, while vectorization avoids repeated four-dimensional PSF indexing. The method differs from TDOA-aided NF-SPICE by directly reconstructing a spatial image without a pre-estimated source range, although a scan region and array-geometry model remain necessary.

The simulation verifies single- and coherent double-source reconstruction. The shared 950 Hz tank data demonstrate separation of sources merged by conventional beamforming, an approximately 60% reduction in −3 dB mainlobe width, more than 10 dB peak-sidelobe improvement, and representative reconstructed range errors below 0.2 m. The Danjiangkou experiment extends the evaluation to a moving UUV using 51 channels from a 1-km lakebed-fiber deployment, a 4 kHz sampling rate, and an 800–840 Hz processing band. The lake result is qualitative because synchronized underwater trajectory and exact cable geometry are unavailable. Future work will focus on adaptive PSF calibration, quantitative UUV trajectory comparison, robustness to cable deformation and sound-speed mismatch, and measured runtime gains under different spatial-resampling factors.

Acknowledgments

This work was supported by the National Key Research and Development Program of China under Grant 2025YFE0214800 and the China Postdoctoral Science Foundation under Grant 2025M780261.

References

[1] M. P. A. van den Ende and J.-P. Ampuero, "Evaluating seismic beamforming capabilities of distributed acoustic sensing arrays," *Solid Earth*, vol. 12, no. 4, pp. 915–934, 2021.

[2] Y. Yang, T. Xu, S. Feng, J. Huang, and F. Li, "Optical fiber hydrophone based on distributed acoustic sensing," in *Fiber Optic Sensing and Optical Communication*, ser. Proceedings of SPIE, vol. 10849, 2018, pp. 59–63.

[3] N. Shpalensky, L. Shiloh, H. Gabai, and A. Eyal, "Use of distributed acoustic sensing for doppler tracking of moving sources," *Optics Express*, vol. 26, no. 13, pp. 17 690–17 696, 2018.

[4] K. T. Drylerakis, M. Belal, R. Mestre, T. J. Norman, and C. Evers, "Source detection and tracking for underwater distributed acoustic sensing," in *2024 32nd European Signal Processing Conference (EUSIPCO)*, 2024, pp. 1292–1296.

[5] W. H. Richardson, "Bayesian-based iterative method of image restoration," *Journal of the Optical Society of America*, vol. 62, no. 1, pp. 55–59, 1972.

[6] L. B. Lucy, "An iterative technique for the rectification of observed distributions," *The Astronomical Journal*, vol. 79, pp. 745–754, 1974.